Mar. 2012, Volume 6, No. 3 (Serial No. 52), pp. 280-299
Journal of Civil Engineering and Architecture, ISSN 1934-7359, USA

An Application of Damage Detection Methods to A Real World Structure Subjected to Ground Motion Excitation

Francesco Cavalieri[1], Maura Imbimbo[2] and Raimondo Betti[3]

1. Department of Structural Engineering & Geotechnics, Sapienza - University of Rome, Rome 00197, Italy

2. Department of Civil and Mechanical Engineering, University of Cassino, Cassino (FR) 03043, Italy

3. Department of Civil Engineering and Engineering Mechanics, Columbia University, New York NY 10027, USA

Abstract: This paper aims at investigating the efficacy of different state-of-art damage detection methods when applied to *real world* structures subjected to ground motion excitations, for which the literature contributions are, at present, still not fully comprehensive. To this purpose the paper analyses two test structures: (1) a four-story scaled steel frame tested on a shake table in a controlled laboratory conditions, and (2) a seven-story reinforced concrete building monitored during the seismic excitations of the 1999 Chi-Chi (Taiwan) Earthquake main shock and numerous fore and aftershocks. Some model based damage approaches and statistics based damage indexes are reviewed. The different methodologies and indexes are, then, applied to the two test structures with the final aim of analysing their performance and validity within the case of a laboratory scaled model and a *real world* structure subjected to input ground motion.

Key words: Identification, damage, model, statistical, data-driven.

1. Introduction

At present many damage detection methodologies have been proposed in the scientific literature. One traditional approach is to compare the behaviour of the structure in its undamaged and damaged states and look at changes that occur in its dynamic characteristics (e.g., natural frequencies, damping ratios, mode shapes) and/or response. In carrying on this comparison, mathematical and/or physical models that represent the structure in its undamaged and damaged states must be identified and this can be accomplished following different approaches. As an example, Friswell et al. [17] proposed to identify modal models of a structure by using a model updating procedure that compares the recorded response of the structure with the predicted response derived from an iteratively updated finite element model. Others approaches use dynamic measurements of the structural input and/or output to identify a mathematical, not necessarily physical, “black box” model of the structure that properly maps inputs and outputs. Among them, Brinker et al. [7] performed, in the frequency domain, the identification of the modal characteristics of a structure using the Frequency Domain Decomposition (FDD) applied in the cases of known or unknown input, while Juang [24] proposed, in the time domain, the OKID (Observer Kalman/filter Identification) — ERA/DC (Eigensystem Realization Algorithm with Data Correlation) algorithm. Yu at al. [50] analyse the time domain identification of systems with a limited number of instrumentation measurements. Pati et al. [36] used the rational wavelets. Bai and Keller [4] conducted dynamic experiments on a GFRP composite pedestrian bridge, retrieving its modal parameters in the time and frequency domain by applying two output-only techniques. In their study, Moaveni et al. [31] validated and cross-checked the results derived from the application of six system identification algorithms, including three output-only and three input-output methods, with reference to a

Corresponding author: Maura Imbimbo, Ph.D., associate professor, research fields: structural health monitoring, system identification, strengthening of structures with FRP. E-mail: mimbimbo@unicas.it.

full-scale seven-story reinforced concrete building slice, tested on the unidirectional UCSD-NEES shake table. The three output-only methods used in this work were successfully applied by He et al. [20] the dynamic field test data from the Alfred Zampa Memorial Bridge. Fraser et al. [16] developed an automated modal analysis procedure to apply output-only identification techniques for continuous health monitoring and therefore a real-time data transmission. Saitta et al. [39] studied the application of feature selection to system identification, while Kerschen et al. [25] presented a review of the past and recent developments in system identification of nonlinear structures.

On the direct use of vibration measurements to locate and quantify damaged areas in a structural system, an exhaustive literature review on frequency domain methods for damage detection can be found in Doebling et al. [13, 14]. Alvandi and Cremona [2] reviewed some of the most common Vibration-Based Damage Detection (VBDD) techniques, based on changes of mode shapes and/or modal frequencies. Cruz and Salgado [11] tested the performance of various model based and data-driven methods in detecting damage on a composite (steel/RC) bridge and a RC bridge. The novel approach for vibration-based damage detection proposed by Deraemaeker and Preumont [12] relies on the use of a large network of sensors to which a programmable linear combiner, working as a modal filter, is attached. Kim et al. [26] presented a damage monitoring scheme to give warning of the occurrence, the location and the severity of damage under temperature-induced uncertainty conditions. Capecchi and Vestroni [8] addressed the issue of understanding when only the natural frequencies are sufficient for damage detection, without computing the mode shapes. He [19] related the damage detection to model updating methods. Staszewski [44] discussed the use of wavelets in structural damage detection problems, while Rucka and Wilde [38] applied the continuous wavelet transform for estimating the damage location in beam and plate structures. The analytical and experimental results of the ASCE benchmark structure were used by Barroso and Rodriguez [5] and Nair at al. [33] to test the efficacy of several algorithms for damage identification and localization. Panigrahi et al. [35] conducted numerical analyses about damage detection in a uniform strength beam using genetic algorithm. The study of Ratcliffe at al. [37] investigated an alternative approach, which relies on the reciprocity theorem and involves the installation on the structure of a large array of low cost MEMS accelerometers. Sakellariou and Fassois [40] introduced a stochastic output error (OE) vibration-based methodology for damage localization and quantification in structures under earthquake excitation. By using a multi-criteria approach, incorporating the modal flexibility and the modal strain energy methods, Shih at al. [43] tried to identify and localize single and multiple damages in numerical models of flexural members having different boundary conditions. The work by Koo et al. [28] presented a vibration-based damage detection method for shear buildings using the damage-induced deflections estimated by modal flexibility obtained from ambient vibration measurements. A new structural damage detection method based on the statistical moments of dynamic responses of a structure has been recently proposed by Xu et al. [48]; the experimental study conducted on three shear-type models showed that the proposed method is sensitive to local structural damage but insensitive to measurement noise. Starting from the Damage Locating Vector (DLV) method proposed by Bernal [6], Jang et al. [23] developed the Strain DLV method, i.e., a method combining DLV and static strain measurements. Wang and Chan [47] reviewed the recent developments in damage detection and condition assessment techniques based on vibration-based damage detection and statistical methods. A sensitivity-based finite element model updating strategy was used by Moaveni et al. [32] to detect, localize and quantify damage in a full-scale seven-story reinforced concrete building slice, tested on the unidirectional UCSD-NEES shake table. In their paper, Yan et al. [49] presented a state-of-art review of damage detection methodologies,

classified into traditional-type and modern-type, the latter taking modern signal processing technique and artificial intelligence as analysis tools. The study by Salawu and Williams [41] presented full-scale vibration tests conducted before and after structural repairs on a multi-span reinforced cement concrete (RCC) highway bridge. They studied the correlations between the different stages of the repair works and the changes in the dynamic characteristics of the bridge. Waheb and Roeck [46] described the results of field vibration tests on three concrete bridges with the aim to correlate finite element models with test results. Other interesting research studies are presented in Koh [27], Liu [30], Kosmatka and Ricles [29], Hermans and Auweraer [21] and Alampalli and Cioara [11], Yu et al. [50, 51].

Among the numerous studies available in the literature about the vibration-based damage detection problem, there are not many applications to real cases. This is an important limiting factor for determining proper damage indexes (either model based or data-driven and/or output-only) since testing them on simulated data could provide false indications about their performance in real applications. The aim of this paper is to provide a contribution to the SHM problem with reference to this last important aspect, by looking at the performance of different state-of-art methodologies and indexes for laboratory scaled models and, especially, for *real world* structures. To this purpose the paper analyses two case studies; in the first one, a four-story scaled steel frame, tested on the shake table at the Columbia University and damaged by changing the stiffness of certain structural elements, is analysed. The second case study is a seven-story reinforced concrete building (of the Civil and Environmental Engineering Department at NCHU) in Taichung (Taiwan) subjected to fore- and aftershocks of the 1999 Chi-Chi Earthquake.

2. Damage Detection Methods

In this section, some model based damage methods and statistics based damage indexes are reviewed. The different methodologies and indexes are, then, applied to the two case studies presented in section 0 with the final aim of analysing their performance and validity within the cases of a laboratory scaled model and a *real world* structure subjected to input ground motion.

2.1 Model Based Damage Indexes

In this section, some damage locating indexes, based on changes that occur in the identified mode shapes, frequencies and stiffness matrices, are presented. Such indexes require the use of two records, one in the undamaged state and one in the damaged state, and assume linear structural behaviour within each single record. One of the most common approaches to assess the presence of damage consists of comparing the natural frequencies of each mode before and after the event causing the potential damage. However, the approach is generally unreliable when dealing with smaller damage levels and with data records with a higher noise level such as the case of real world structures.

2.1.1 Flexibility Change Based Indexes

Another interesting damage index is based on the assumption that a localized damage in a structure causes a decrease in stiffness and, consequently, an increase in flexibility. If two measurement sets are available, one for the undamaged state and one for the damaged state, it is possible to identify the flexibility matrices $\mathbf{F}$ and $\mathbf{F}^d$ for the two states. Considering these two flexibility matrices, Alvin et al. [3] defined two global index vectors, $\mathbf{rdi}_1$ and $\mathbf{rdi}_2$, of dimensions equal to the number of degrees of freedom of the structure, whose values give an estimate of the damage amount and position:

$$\mathbf{rdi}_1 = \left|\mathrm{diag}\left(\mathbf{F}^d - \mathbf{F}\right)\right| ; \mathbf{rdi}_2 = \left|\mathrm{diag}\left(\mathbf{F}^d - \mathbf{F}\right)\right| / \left|\mathrm{diag}\left(\mathbf{F}\right)\right| \quad (1)$$

It is also possible to compute an element based flexibility matrix $\mathbf{F}_e = \boldsymbol{(SL)F(SL)^T}$ for the two states, by using the transformation matrix $\mathbf{SL}$ that links the displacements of the system's dofs and the forces acting on the structure to those relative to the inter-story elements.

Analogously to Eq. (1), two indexes related to the single element rather than the dof can be defined:

$$\mathbf{rdi}_{1,e} = \left|\mathrm{diag}\left(\mathbf{F}_e^d - \mathbf{F}_e\right)\right|;\ \mathbf{rdi}_{2,e} = \left|\mathrm{diag}\left(\mathbf{F}_e^d - \mathbf{F}_e\right)\right| / \left|\mathrm{diag}\left(\mathbf{F}_e\right)\right| \quad (2)$$

Both the global and local flexibility matrices can be computed by using either all the significant modes of the structure or only some of them and, consequently, this will reflect in the indexes defined in Eq. (1) and Eq. (2). This is an important aspect since, in real life applications, only few predominant modes can be identified because of the measurement incompleteness or because higher-order modes are barely excited.

2.1.2 Damage Index Method

Among the model based damage indicators, Stubbs et al. [45] proposed a damage indicator β_j for the *j*-th element, which is computed on the basis of the identified system's stiffness matrix and the mass normalized mode shapes, φ, in both the damaged and undamaged states. These indicators, one for each inter-story element, are then normalized to provide a more robust statistical criterion for damage localization. The normalized indicator for the *j*-th element, z_j (j = 1, 2, ...), is given by:

$$z_j = \frac{\left(\beta_j - \bar{\beta}\right)}{\sigma_\beta} \quad (3)$$

where $\bar{\beta}$ and σ_β are the mean and the standard deviation of all the indicators, respectively.

2.1.3 Modal Strain Energy Change Ratio (MSECR)

This damage index is based on the definition of Modal Strain Energy (MSE) for the *j*-th element and the *i*-th mode that, in the undamaged and damaged states, is represented by the expressions:

$$\mathrm{MSE}_{ij} = \boldsymbol{\varphi}_i^T \mathbf{K}_j \boldsymbol{\varphi}_i;\ \ \mathrm{MSE}_{ij}^d = \boldsymbol{\varphi}_i^{d,T} \mathbf{K}_j \boldsymbol{\varphi}_i^d \quad (4)$$

where $\mathbf{K}_j$ is the stiffness matrix of *j*-th element, obtained by considering only the stiffness of the *j*-th element and setting to zero all the other ones, in the global stiffness matrix, while $\boldsymbol{\varphi}_i$ and $\boldsymbol{\varphi}_i^d$ are the identified *i*-th mode shapes for the two states. Since the location of damage is unknown, the undamaged stiffness matrix of the *j*-th element is used in both the undamaged and the damaged states as an approximation. According to the theory of Shi et al. [42] the Modal Strain Energy Change Ratio (MSECR) for the *j*-th element and the *i*-th mode can be calculated as:

$$\mathrm{MSECR}_j^i = \frac{\left|\mathrm{MSE}_{ij}^d - \mathrm{MSE}_{ij}\right|}{\mathrm{MSE}_{ij}} \quad (5)$$

and by looking at the contributions of the various modes on each single element, a modal strain energy change ratio related to the *j*-th element, msecr_j, can be written as:

$$\mathrm{msecr}_j = \frac{1}{\mathrm{n}} \sum_{i=1}^{\mathrm{n}} \frac{\mathrm{MSECR}_j^i}{\mathrm{MSECR}_{max}^i} \quad (6)$$

where MSECR_{max}^i is the largest value for each mode while n indicates the number of modes used in the analysis. In using this index, damage appears to be located in correspondence of those elements that show the largest values of such an index.

2.2 Statistics Based Damage Indexes

In the context of the statistical pattern recognition, the process of vibration-based damage detection relies on the analysis only of the recorded output signals. One of the most thorough review of the statistics approach is provided by the work of Fugate et al. [18], where the different phases are outlined and discussed. After the phase of data acquisition and cleansing, the collected output data are used in the feature extraction phase which consists of evaluating damage sensitive parameters and/or functions, e.g., the residuals between the observed and predicted records. In the case of supervised algorithm, which is the one used in this work, the data are available for both the undamaged and the damaged structures. The key phase of the statistics approach consists of developing statistical algorithms able to analyse the distributions of the extracted damage sensitive features and, eventually, their changes occurred in case of damage from the undamaged to the damaged states with the aim of detecting the presence and location of damage. For example, the mean, the variance and others functions of the damage sensitive features are

monitored through control charts to trace (pinpoint) any change over time.

The statistical process control allows also to minimizing false indications of damage. In fact, the output acceleration measurements derived from experimental tests are somewhat correlated. The degree of autocorrelation can lead to control charts that might provide some false alarms or might fail to indicate when the selected parameters/features change significantly from the undamaged case to the damaged case. Following the study [18], a solution to this drawback consists of working with the residuals between the observed data and those obtained from fitting an autoregressive (AR) model to the observed data. If the fitted AR model is set correctly, the residuals appear uncorrelated without systematic patterns.

Some control charts can be constructed using the residuals directly as data. Fugate et al. [18] suggest to construct X-bar and S control charts and, in this paper, it is also defined the R control chart. To detect changes in the residuals, it is necessary to manipulate them, e.g., to form subgroups, compute a function of the residuals within each subgroup and chart it. The subgroups, of size n, are chosen on the basis of similar observations within them. If n is too large, a drift in the mean value can be possibly averaged-out and so not easily detectable. Several studies proved that in most cases the best choice for the subgroup size is 4.

In applying the supervised statistical algorithms, the AR model parameters and the chart control limits are first computed on the basis of the undamaged data. Then, the new acceleration measurements from the possibly damaged structure can be predicted using the new data and the undamaged AR model parameters. New residuals can be determined and charted. If damage occurs before the new set of data, the AR model should not fit well the new acceleration measurements and a statistically significant number of residuals should fall beyond the chart control limits, denoting the presence of damage.

3. Performance of the Damage Detection Methods Applied to Two Case Studies

With the purpose of evaluating the performance of the different state-of-art methodologies and indexes discussed in the previous section for laboratory scaled models and, especially, for *real world* structures, this section analyses two case studies: (1) a four-story scaled steel frame, tested on the shake table at the Columbia University and damaged by changing the stiffness of certain structural elements; (2) a seven-story reinforced concrete building (of the Civil and Environmental Engineering Department at NCHU) in Taichung (Taiwan) subjected to fore- and aftershocks of the 1999 Chi-Chi Earthquake.

3.1 Damage Detection in a Laboratory Structure: A Four-Story Scaled Steel Frame

3.1.1 Description of the Structure

The first structure analysed in this study is the four-story A36 steel frame shown in Fig. 1.

The inter-story height is 533 mm and the floor plate dimensions are 610×457×12.7 mm. The floors are braced diagonally only in one direction (strong), while in the

Fig. 1 Tested four-story frame.

other (weak) direction they remain unbraced. The columns have cross-sectional dimensions of 50.8×9.5 mm while the cross-section of the diagonal braces is 50.8×6.4 mm. All the structural connections are bolted. The frame is mounted on an ANCO uni-axial hydraulic shake table, with a 1.5×1.5 m platform, which provides an excitation along the weak direction in the frequency range of about 0 to 150 Hz with a peak acceleration of 3 g. The model is instrumented with piezoelectric accelerometers, with seven channels of acceleration response on the structural model and one reference channel (representing the input) on the shake table's platform. The sensor locations are chosen in order to capture the three-dimensional behaviour of the structure, caused either by the excitation or by the frame's asymmetry. The data acquisition scheme is shown in Table 1.

Damage is simulated by introducing a 66% reduction of the cross-section of one column between the 2nd and 3rd floors (see the circle in Fig. 1), inducing a 22.2% reduction of the interstory stiffness between these two floors in the weak bending direction. Hereafter, the undamaged or Reference Case will be referred to as RC while DC will indicate the Damaged Case. Although the uniaxial excitation along the weak direction, the response of the frame was characterised by accelerations along both the weak and the strong directions, the last ones due to some structural imperfections in the RC case and to the presence of damage in the DC case. However in this paper, for damage detection analysis, the frame is represented as a two-dimensional shear-type model in the weak direction, as already studied in Fraraccio et al. [15] Consequently, only the signals recorded by the channels 2, 3, 4 and 5 are considered (see the arrows in Fig. 1 While the channels 6 and 7, set along the strong direction, and the channel 8, useful to detect the torsional behaviour of the 4th floor, are not included. See Table 2 for the list of the registered channels.

Table 1 Data acquisition scheme.

CH	Sensor position	Orientation
1	Table reference	Weak
2	1st floor	Weak
3	2nd floor	Weak
4	3rd floor	Weak
5	4th floor	Weak
6	3rd floor	Strong
7	4th floor	Strong
8	4th floor	Weak

Table 2 Scheme of used channels and correspondent dofs.

Orientation	Registered Channel	Dof
Weak	2	1
Weak	3	2
Weak	4	3
Weak	5	4

In Cavalieri et al. [9], this frame was identified by applying the time domain Observer Kalman filter Identification (OKID) algorithm, using the time histories of both input and output, and the frequency-domain Enhanced Frequency Domain Decomposition (EFDD) with output-only information. The two approaches provided the same results in terms of identified natural frequencies, damping ratios and undamped mode shapes, results that are shown in Tables 3–4.

From the analysis of the four identified modes, it is clear that these modes correspond to the four bending modes along the weak direction of the frame.

Table 3 Identification results for the RC case.

RC CASE			
Mode I	Mode II	Mode III	Mode IV
Undamped mode shapes			
0.235	0.523	0.771	0.608
0.465	0.616	0.037	-0.707
0.530	0.100	-0.486	0.307
0.668	-0.580	0.410	-0.188
Eigenfrequencies [Hz]			
3.902	10.980	18.645	26.243
Modal Damping Ratios			
0.003	0.004	0.004	0.006

Table 4 Identification results for the DC case.

DC CASE			
Mode I	Mode II	Mode III	Mode IV
Undamped mode shapes			
0.229	0.526	0.724	0.603
0.452	0.629	0.059	-0.730
0.543	0.082	-0.541	0.204
0.670	-0.566	0.424	-0.252
Eigenfrequencies [Hz]			
3.856	10.808	18.327	25.442
Modal Damping Ratios			
0.003	0.003	0.004	0.005

3.1.2 Model Based Damage Indexes

Fig. 2a and Fig. 2b show the flexibility change based indexes $\mathbf{rdi}_{1,e}$ and $\mathbf{rdi}_{1}$, respectively, for different numbers of identified modes (1, 2, 3 and the complete set (4)). In Fig. 2a, the $\mathbf{rdi}_{1,e}$ index, although showing non-zero values in all the elements, reaches its highest value in correspondence of the 3rd element in all the graphs. It is in correspondence of such element that there is the 22% reduction of inter-story stiffness. Similar conclusions can be derived from Fig. 2b for the $\mathbf{rdi}_{1}$ index: also in this case the largest value is always reached along the 3rd dof in all of the graphs. Both **rdi** indexes, at the degree of freedom or at the element level, show that the value corresponding to the third dof or element is the highest among the other values, indicating substantial changes in the flexibility at that location. Hence, it can be concluded that these two indexes provide a clear indication about the damage position for the simple laboratory structure considered in this study. However, they do not allow to quantify the amount of structural damage: in fact, looking at the numerical values of such indexes, there is no correlation to the 22% inter-story stiffness reduction. Identical conclusions can be derived for the others flexibility change indexes $\mathbf{rdi}_{2,e}$ and $\mathbf{rdi}_{2}$ described in section 0, as shown in Fig. 3a and Fig. 3b.

From the analysis of the $\mathbf{rdi}_{2,e}$ and $\mathbf{rdi}_{2}$ indexes, it is again possible to estimate the damage position in the frame

Fig. 4 shows the plot of the values of z_j given by Eq. (3) as a function of the inter-story element for the laboratory frame. In the ideal case of noise free signals, the z_j values should be larger for the elements where damage occurs while they should be close to zero for the elements indirectly affected by damage. In this way, it should be possible to easily localize the areas of structural damage.

For real noisy signals, this distinction in the z_j values is less evident, with lower values that could be even negative: this is mainly due to the presence of noise in the measurements. However, the gap between z_j values corresponding to elements with damage and those

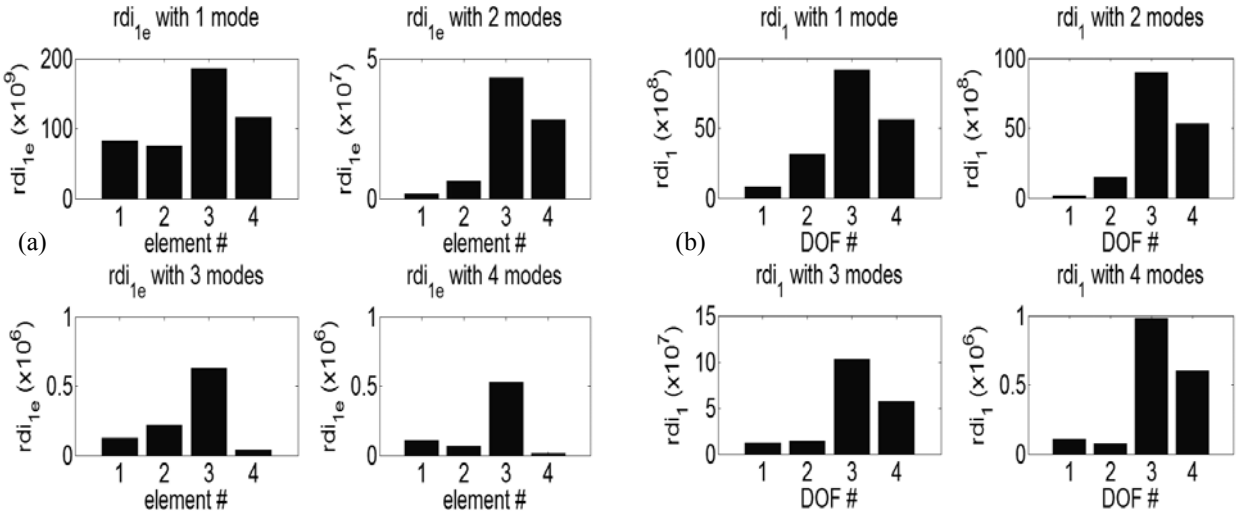

Fig. 2 (a) $\mathbf{rdi}_{1,e}$ plots and (b) $\mathbf{rdi}_{1}$ plots, with different numbers of identified modes.

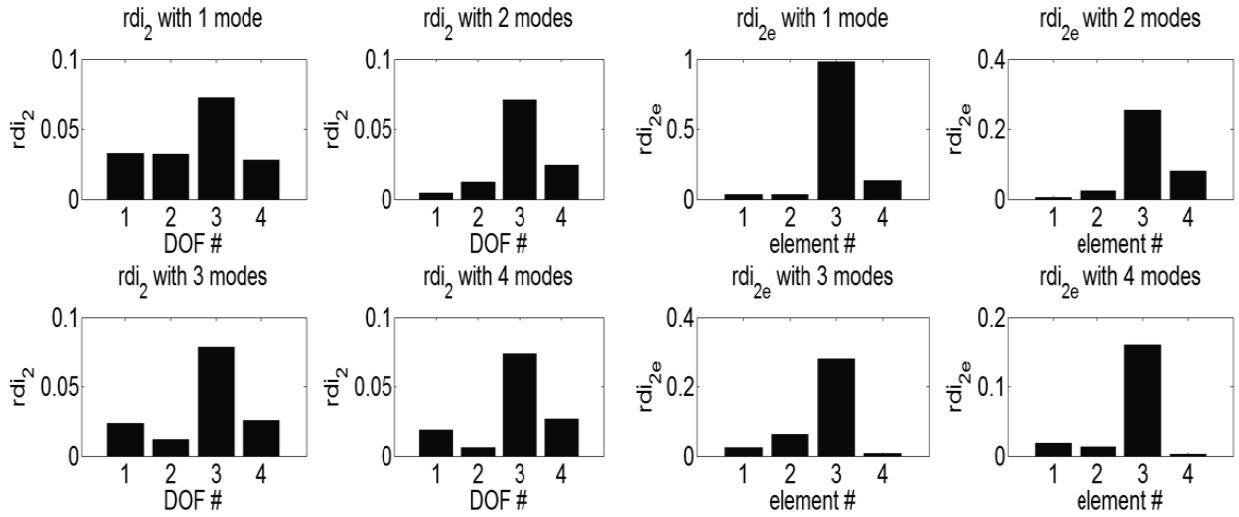

Fig. 3 (a) $rdi_{2,e}$ plots and (b) rdi_2 plots, with different numbers of identified modes.

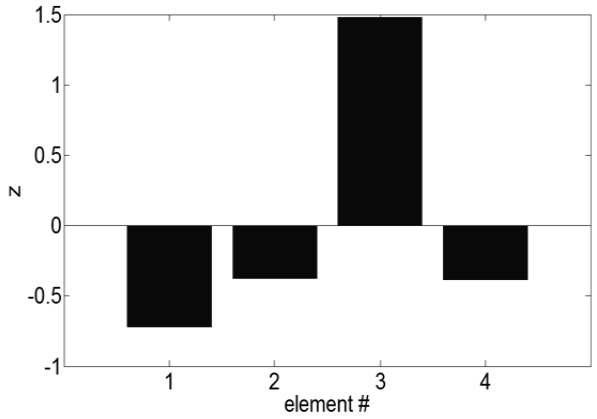

Fig. 4 z plot.

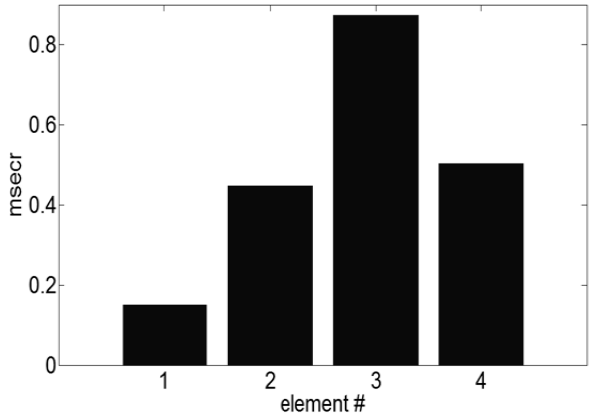

Fig. 5 Mserc plot.

without damage should be still large, with the damaged elements showing the largest positive values of z_j. In Fig. 4, the z_j values are plotted for the case of the laboratory frame. It is shown that the highest value, as well as the sole positive value, is reached on the 3rd inter-story element, which corresponds to the location where damage is occurred. However, as for the previous indexes, no indication can be given about the amount of structural damage (in this case 22% reduction of the floor stiffness).

Fig. 5 shows the modal strain energy ratio **msecr**, given by Eq. (6), as a function of the inter-story element for the shear-type model of the laboratory frame considered in this study.

Although all elements have non-zero values, the highest value is reached along the 3rd element where damage is induced. The values associated with the second and forth inter-story elements are also somewhat affected by the presence of the damage on the third floor: in fact, they show not negligible values of msecr. Element 1 shows the least effect from the structural damage. However, from the numerical values obtained, no indication on the amount of damage (22% reduction of the 3rd floor stiffness) can be obtained.

Similarly to the other previous indexes, this result confirms the applicability of such an index to locate areas of damage within a structural system but also its

incapacity in providing any quantification of the amount of damage occurred.

3.1.3 Statistics Based Damage Indexes

Fig. 6a and Fig. 6b show the autocorrelation functions, respectively for all the output signals and for the residuals computed by an AR(1500) model, in the undamaged state. The AR coefficients are estimated by the Yule-Walker method and the model order is chosen equal to 1500. It can be seen that the autocorrelation for all the residuals quickly decreases and approaches zero after few time lags. Similar results are obtained for the DC case.

In these analyses, the three control charts (X-bar, S and R) are based on 1850 subgroups of size 4.

- X-bar control chart

The X-bar control charts of the residuals for the 4 channels on the laboratory frame are presented in Fig. 7a and Fig. 7b for the undamaged and damaged cases, respectively. For the case of the X-bar chart, the sample means μ within each subgroup are computed and charted. The centreline of the chart is the sample mean of the charted values and, after the normalization, is equal to 0. The sample variance of each subgroup is first determined and then these variances are averaged to give a pooled estimate of the variance. A simple average is appropriate because each subgroup is of size 4. The square root of the pooled variance, s_p, is used as an estimate of the population standard deviation. The Upper and Lower Control Limits, UCL and LCL, are given by $(0 \pm z_\alpha s_p/\sqrt{n})$ where n = 4 and z_α represents the α quantile of the standard normal distribution. In this paper, α is chosen 0.005.

In Fig. 7a and Fig. 7b, the centreline and the control limits are indicated with three horizontal lines. The outliers, marked by a "∗", correspond to the subgroup sample means which fall outside the control limits. For the RC case, approximately 19 charted values (i.e., 2α = 1% of total 1850 samples) are out of the control limits. On the contrary, in the DC case, a greater and statistically significant number of outliers (around 5% of total samples) is detected; this change indicates the presence of structural damage in the frame.

With the aim of detecting the damage position in the frame, for each channel, the deviations between the upper outliers and the UCL and those between the lower outliers and the LCL are collected in a vector, for the RC and DC cases. Then, the root mean square (rms) of these vectors is computed and plotted in Fig. 8, where each single dof corresponds to a channel. The figure shows that the highest rms values for the DC case are reached along the 2nd and 3rd dofs, as well as the highest variations between the RC and DC cases, confirming that the damage is located between the 2nd and 3rd floors.

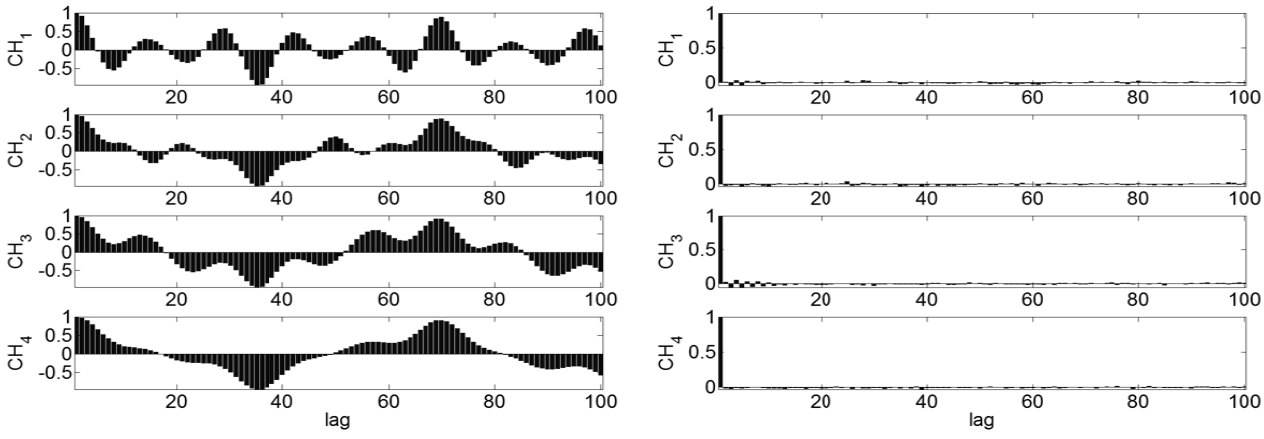

(a) (b)

Fig. 6 Autocorrelation functions in the RC case: (a) for the output signals; (b) for the residuals.

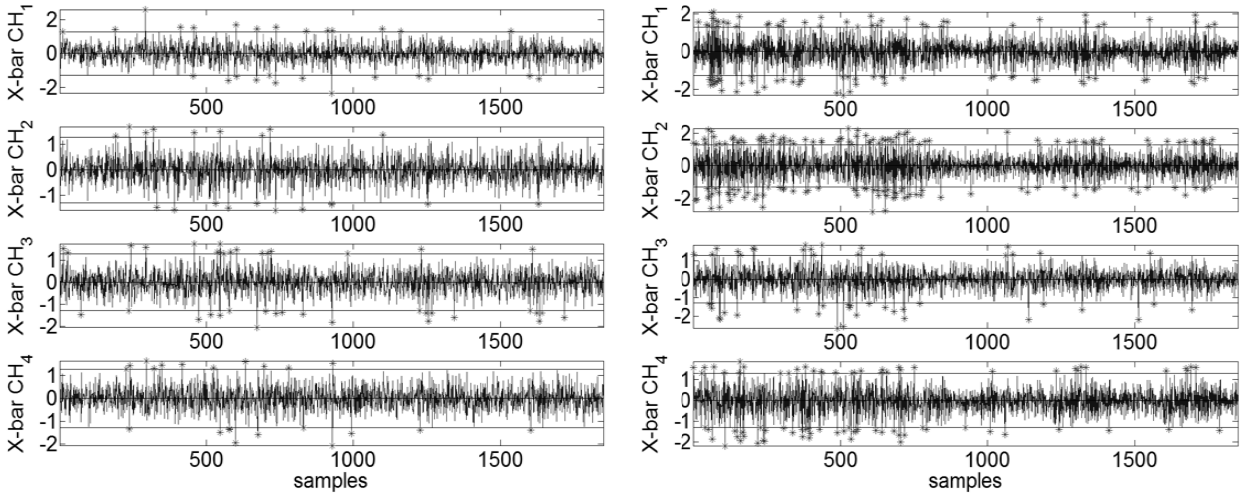

Fig. 7 X-bar control charts for the residuals: (a) RC case; (b) DC case.

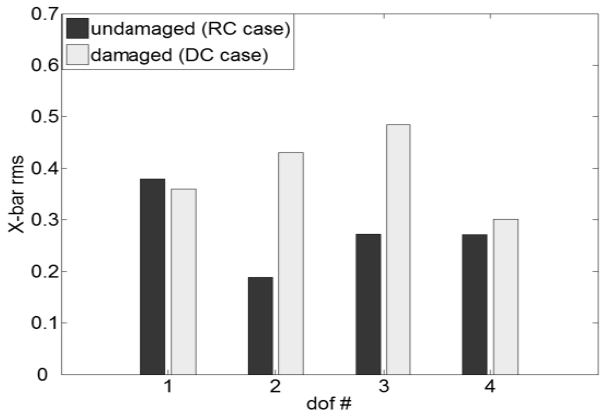

Fig. 8 Rms values computed for each dof on the X-bar charts, in the RC case and DC case

- S control chart

Another chart which can be used to monitor the variability within each subgroup is the S control chart. The main difference with the X-bar chart is that now, for each subgroup, the sample standard deviation of the (normalized) residuals is computed and charted, rather than the mean. The centreline of the chart is the sample mean of the charted values, while the upper and lower control limits are:

$$\mathrm{UCL} = \bar{S}\sqrt{\frac{\chi^2_{1-\alpha,n-1}}{n-1}};\quad \mathrm{LCL} = \bar{S}\sqrt{\frac{\chi^2_{\alpha,n-1}}{n-1}} \qquad (7)$$

Where α is chosen to be 0.005, n = 4, $\chi^2_{p,n}$ is the p-th quantile of a Chi-square random variable with n degrees of freedom and $\bar{S}$ is the average of the charted standard deviations. The S charts for all the channels show the same properties of the X-bar charts and are not reported here. For each S chart, the deviations between the upper outliers and the UCL and those between the lower outliers and the LCL are collected in 4 different vectors (one per signal), whose root mean squares are computed and plotted in Fig. 9. This figure shows that the highest rms values for the DC case, as well as the highest gaps between the RC and the DC cases, are reached along the 2nd and 3rd dofs, confirming the finding that damage is located between the 2nd and 3rd floors. This result is analogous to the one obtained with the X-bar control chart. However, in Fig. 9, a high variation from RC to

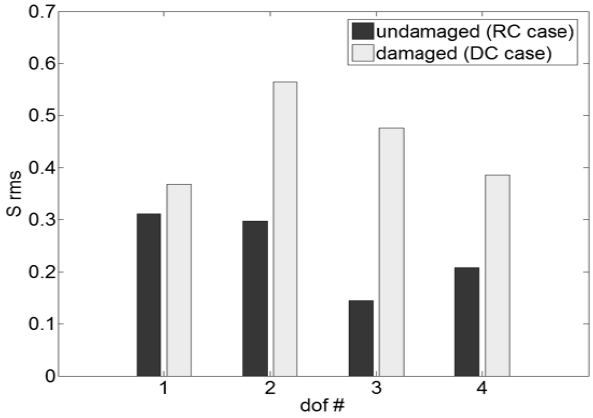

Fig. 9 Rms values computed for each dof on the S charts, in the RC case and DC case.

DC can also be observed along the 4th dof where, instead, no damage has occurred and this makes the S rms approach less reliable than the X-bar chart.

- R control chart

An alternative chart, defined in this study, is the R control chart. For each subgroup, the sample range of the (normalized) residuals is computed and charted. This range represents the difference between the maximum and minimum values of a subgroup. The centreline of the chart is again the sample mean of the charted values, while the upper and lower control limits are given as $\pm 3 \sigma / \sqrt{n}$, where $n = 4$ and σ is the standard deviation of the charted values. For brevity, the R charts for all the channels are not reported here: they are no longer linked to $\alpha = 0.005$ and show many outliers in the RC case and even more in the DC case.

For all the R charts, the root mean square of the deviations is computed and plotted in Fig. 10. The results are quite similar to those obtained for the S chart with the highest gaps between the RC and the DC cases along the 2nd and 3rd dofs. However, high rms values and variations from RC to DC can be observed also along the other dofs, where no damage has occurred, and this makes the R rms approach not reliable in localizing the damage in the laboratory frame.

- False-positive testing

In some cases, the monitoring system indicates the presence of damage even when no damage has occurred,

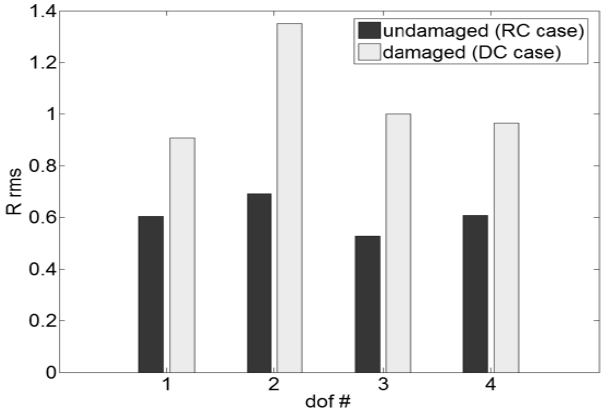

Fig. 10 Rms values computed for each dof on the R charts, in the RC case and DC case.

providing a false-positive indication of the damage. To check the robustness of the control charts, a false-positive test is run, starting by dividing the undamaged output signals into two parts. Then, for each channel, the Statistical Process Control is performed by using the first half of the data measurements as the undamaged time series while the second half is used as the damaged signal and represents the test signal. An AR model is first fitted to the first half of the data set to estimate the AR coefficients: once these coefficients are determined, then the first and second halves of the data series are predicted using the same identified AR model. Residuals are computed for both sets of the data. The model order and the number of subgroups are chosen to be 500 and 2, respectively, to take into account the reduced size of the signals.

Fig. 11a, Fig. 11b and Fig. 11c show the rms of the deviations for the X-bar, S and R charts, respectively, for each dof and for the first and the second half of the data sets. These graphs look different from those presented in Figs. 8–10: in fact, in Fig. 11 the difference between the two bars is in average quite small (an indication that these approaches recognize that the signals are from the same data set) and can be considered related to the natural variability of the experimental data. This result confirms that all three charts are robust against false-positive indications of damage.

3.2 Damage Detection in A Real World Structure: The CEED Building at NCHU

3.2.1 Description of the Structure

The second case study considered in this paper is the building of the Civil and Environmental Engineering Department (CEED) at the National Chung Hsing University (NCHU) in Taichung, Taiwan. This is a seven-story reinforced concrete building, with a basement and a roof floor, with a smaller three-story unit connected along the short side. The base dimensions of the main building are 57 m × 37.5 m, with a height of 26.8 m above ground. This structure was subjected,

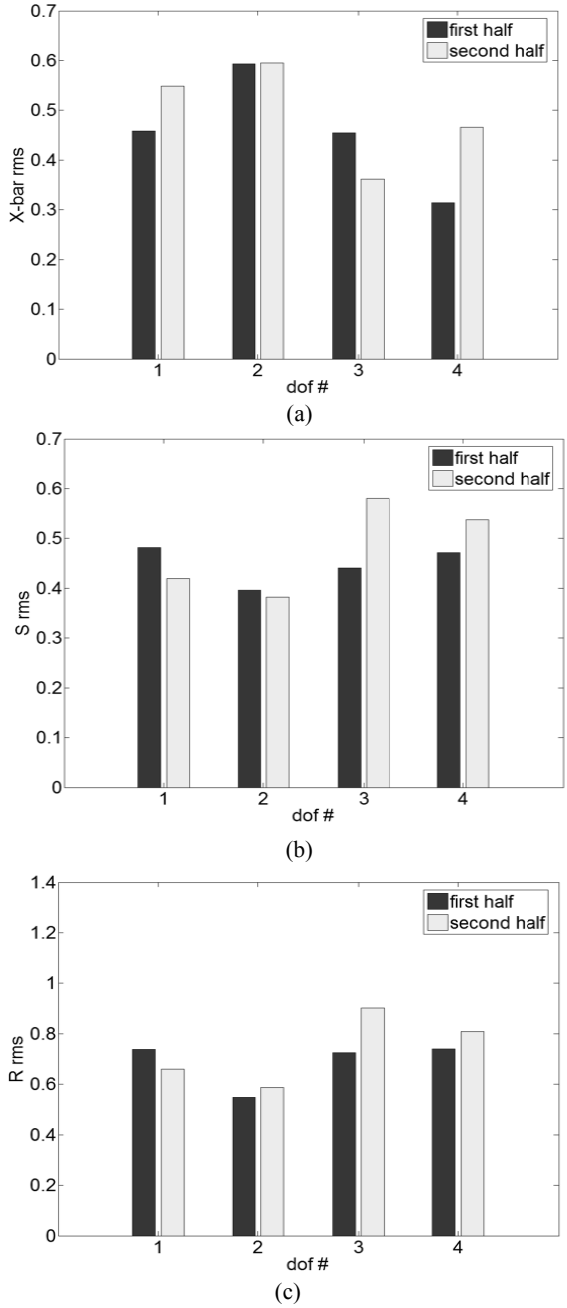

Fig. 11 Rms values computed for each dof, for the first and the second half: (a) X-bar charts; (b) S charts; (c) R charts.

between July 1998 and November 1999, to the Taiwan Chi-Chi Earthquake main shock and numerous foreshocks and aftershocks, and experienced moderate structural damage, including the damage of partition walls and the separation of walls from columns and floor beams in the lower stories. This building was instrumented in 1990 for strong motion monitoring with 29 accelerometers, the locations of which are shown in Fig. 12: eight sensors on the basement, six on the ground level, six on the 4th floor, six on the roof, and three on the free field (E-W, N-S and Up-Down directions), at a location far from the building, which can be considered representative of the free-field ground motion.

In this study, since the interest is focused on the main seven-story building, the structural responses recorded at the eight sensors located in the x- and y-direction on the 4th floor (Channels 12, 13, 14 and 15) and roof (Channels 18, 19, 21, 22), are used as output set. For simplicity, in the next sections of the paper, the registered channels are named as the "dof" labels reported in Table 5.

The time histories recorded at the four sensors located in the x- and y-direction on the first floor (Ch 24, 25, 26, 27), if considered as outputs, do not provide any additional valuable information in terms of global behaviour of the building and, hence, were not included in the output sets. The input set is represented by the acceleration time histories measured by the eight sensors at the basement.

This choice of selection of inputs and outputs, already adopted in Hong et al. [22] as "Flexible Base" Analysis (FBA), allows us to account for the flexibility of the foundation mat and to filter out the soil-structure interaction effects from the identification process. Among the available data sets, the 07/07/1999 and 10/19/1999 recorded signals (small energy foreshock and aftershock, corresponding to the pre- and after-damage states, respectively) have been used for the application of the model based indexes and the statistical approaches. Analogously to the laboratory frame, the undamaged or reference case will be indicated with RC, while the damaged one with DC.

In Cavalieri et al. [10], the study conducted about the dynamic identification and damage detection of the building is presented. In particular, two structural identification techniques, the OKID (Observer Kalman/filter Identification) — ERA/DC (Eigensystem

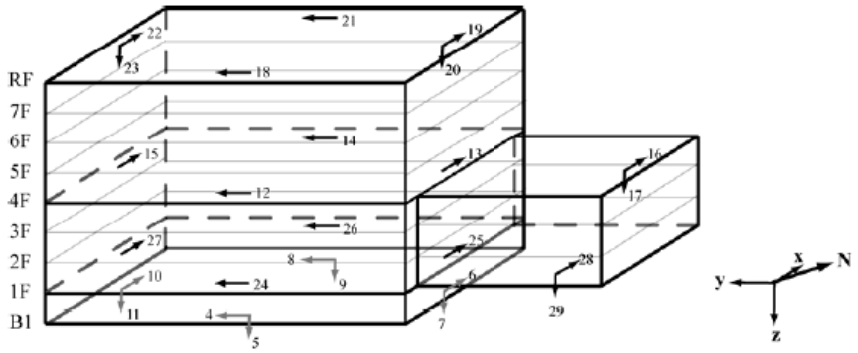

Location	Number of channels
Roof floor	6 (2EW, 2NS, 2V)
Fourth floor	6 (2EW, 3NS, 1V)
Ground level	6 (2EW, 3NS, 1V)
Basement	8 (2EW, 2NS, 4V)
Free field	3 (1EW, 1NS, 1V)
Total	29

Fig. 12 Scheme of the instrumentation set up at the CEE building.

Table 5 Scheme of channels used as output set and correspondent dofs.

Floor	Direction	Registered Channel	dof	Registered Channel	dof
4th floor	x	13	2	15	4
4th floor	y	12	1	14	3
Roof	x	19	6	22	8
Roof	y	18	5	21	7

Realization Algorithm with Data Correlation) algorithm, proposed by Juang [24], and the FDD frequency domain method have been applied. The results derived from OKID-ERA/DC, in terms of identified natural frequencies, damping ratios and undamped mode shapes, agree with those obtained with FDD and are shown in Table 6.

3.2.2 Model Based Damage Indexes

Among the model based damage indexes discussed in section 0, only those based on flexibility changes have been applied to this case study, since the other indexes did not provide interesting results. Fig. 13a and Fig. 13b show the plots of the $\mathbf{rdi}_1$ and $\mathbf{rdi}_2$ indexes, computed using Eq. (1) and including all the available identified modes. It appears that all the monitored dofs have non-zero values. In particular, in the $\mathbf{rdi}_1$ plot the highest values are reached along the 1st, 3rd and 4th dofs, for the 4th floor, and the 5th, 7th and 8th dofs, for the roof. The same can be said for the $\mathbf{rdi}_2$ plot. By looking at the relative values between these two plots, it can be concluded that the building is most damaged along the y-direction, but nothing can be said about the exact position of damage.

An indication about the damage location can be obtained by looking at the difference between the identified flexibility matrices $\mathbf{F}$ and $\mathbf{F}^d$ for the two states. Looking at the matrix $\mathbf{\Delta F} = (\mathbf{F} - \mathbf{F}^d)$, Pandey et al. [34] proposed, for each translational degree of freedom i, a δ_i index defined as the maximum absolute value of the elements in the corresponding row of $\mathbf{\Delta F}$, i.e., $\delta_i = \max_j \left|\Delta F_{ij}\right|$. The damage can be considered located where a large step in the δ_i plot appears.

Fig. 14 shows the $\boldsymbol{\delta}$ plot for the analysed building: in this plot, it is clear that the largest steps, indicated by arrows in the figure, appear between the 1st and 2nd dofs, and the 2nd and 3rd dofs, for the 4th floor, and between the 5th and 6th dofs, and the 6th and 7th dofs, for the roof. Considering that 1st and 2nd, and 5th and 7th are dofs along the y direction — respectively in the 4th floor and roof — it can be observed that the major damage in the building is in the y-direction.

3.2.3 Statistics Based Damage Indexes

The statistics based damage indexes discussed in section 2 are now applied to this case study. Fig. 15 and Fig. 16 show the autocorrelation functions for all the output signals (Fig. 15) and for the residuals computed by

Table 6 Identification results from OKID-ERA/DC.

RC CASE						DC CASE					
I	II	III	IV	V	VI	I	II	III	IV	V	VI
Undamped mode shapes						Undamped mode shapes					
0.263	0.212	0.114	0.042	0.453	0.089	0.319	0.080	0.111	0.444	0.061	0.157
0.068	0.086	-0.250	-0.312	0.067	0.463	0.026	0.098	-0.285	0.046	0.233	-0.466
0.237	-0.129	-0.092	-0.107	0.522	-0.168	0.310	-0.072	-0.100	0.573	-0.057	-0.232
0.226	0.324	0.194	0.637	-0.068	0.510	0.022	0.415	0.161	0.040	0.626	0.475
0.534	0.456	0.317	-0.073	-0.426	-0.176	0.609	0.194	0.284	-0.417	-0.124	-0.208
0.174	0.251	-0.661	0.416	-0.145	-0.403	0.062	0.215	-0.711	-0.059	-0.401	0.435
0.523	-0.285	-0.305	0.155	-0.545	0.225	0.651	-0.155	-0.336	-0.541	0.101	0.249
0.479	0.688	0.499	-0.530	0.113	-0.496	0.038	0.836	0.415	0.035	-0.600	-0.429
Eigenfrequencies [Hz]						Eigenfrequencies [Hz]					
3.084	3.112	3.908	8.598	9.295	10.978	2.239	2.548	3.212	6.938	8.076	9.668
Modal Damping Ratios						Modal Damping Ratios					
0.032	0.021	0.018	0.017	0.016	0.015	0.024	0.022	0.016	0.030	0.033	0.025

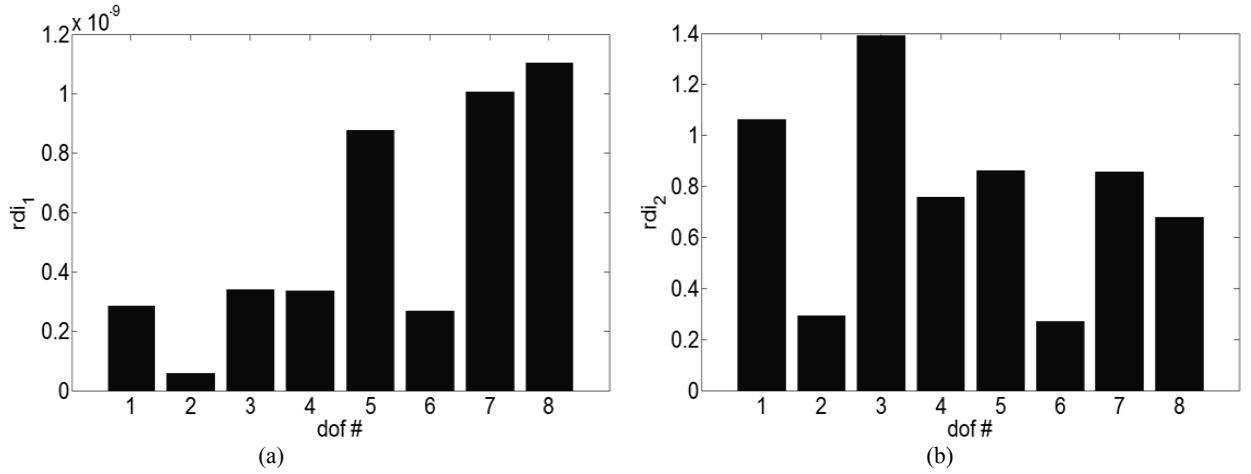

(a) (b)

Fig. 13 (a) rdi$_1$ plot; (b) rdi$_2$ plot.

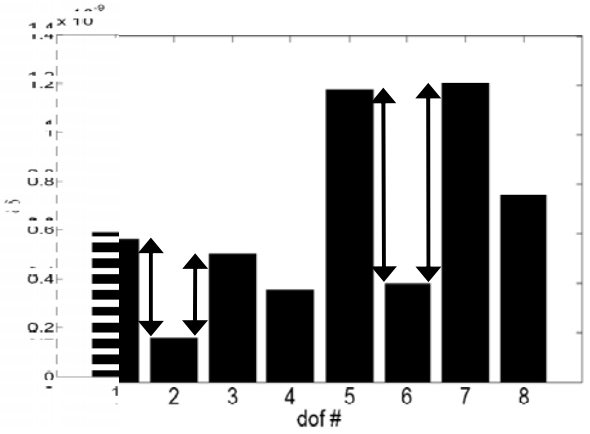

Fig. 14 δ plot.

an AR(1500) model (Fig. 16), for the case of the building in its undamaged state. It can be seen that with p = 1500 the autocorrelation for all the residuals quickly decreases and approaches zero after few time lags, confirming the uncorrelated nature of the residuals.

Similar results have been obtained from the data analysis of the time histories of the response for the building in its damaged condition (DC case). For the reference or undamaged case, the time histories corresponding to the 07/07/1999 ground shaking are used while the structural response recorded during the

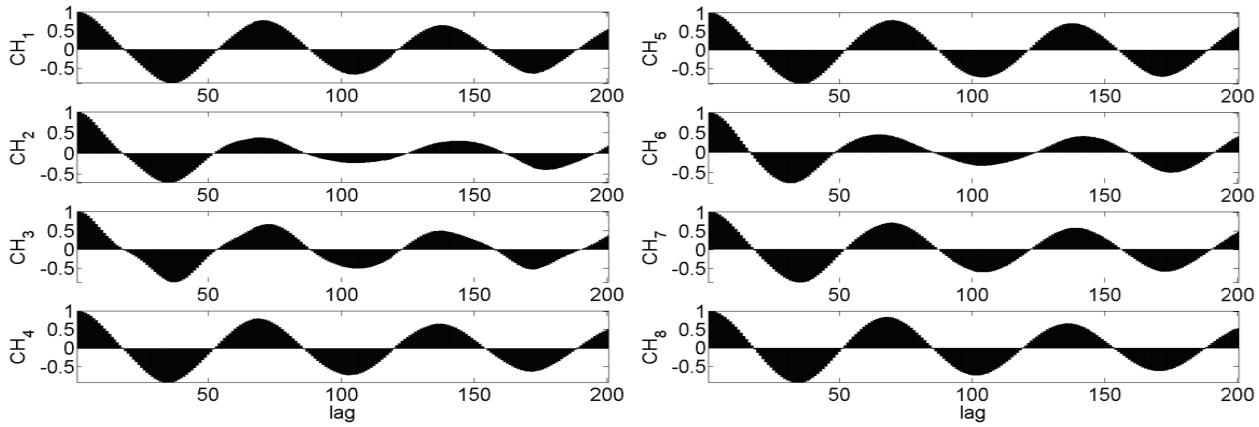

Fig. 15 Autocorrelation functions in the RC case for the output signals.

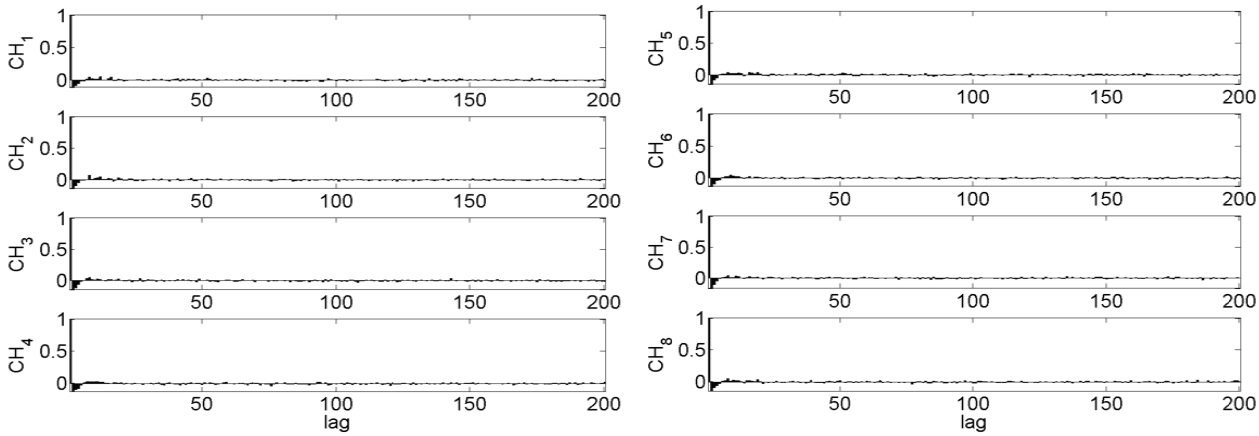

Fig. 16 Autocorrelation functions in the RC case for the residuals.

10/19/1999 earthquake is used as representative of the post-damage scenario (damaged case). In these analyses, the three control charts (X-bar, S and R) are based on 628 subgroups of size 10, while α is chosen 0.005.

- X-bar control chart

Fig. 17 and Fig. 18 show the X-bar control chart for all the residuals, in the undamaged and damaged states, respectively. The centreline and the control limits are indicated with three horizontal lines. The outliers, marked by a "*", correspond to the subgroup sample means which fall outside the control limits.

For the RC case, approximately 6 charted values (i.e., 2α = 1% of total 628 samples) are out of the control limits. On the contrary, in the DC case, a much greater and statistically significant number of outliers (around 6% of total samples) is detected indicating the presence of structural damage.

With the aim of detecting the damage position in the building, for each channel, the deviations between the upper outliers and the UCL and those between the lower outliers and the LCL are collected in a vector for each of the two cases (RC and DC cases). The root mean square (rms) of these vectors is computed and plotted in Fig. 19, where each single dof corresponds to a channel, for both the RC case and the DC case.

It is clear that the highest rms values for the DC case are reached along the 1st and 3rd dofs, for the 4th floor, and the 5th and 7th dofs, for the roof. For these dofs, the gap between the rms values in the DC and RC cases is higher than the corresponding values for the remaining dofs, although significantly high values and gaps can also

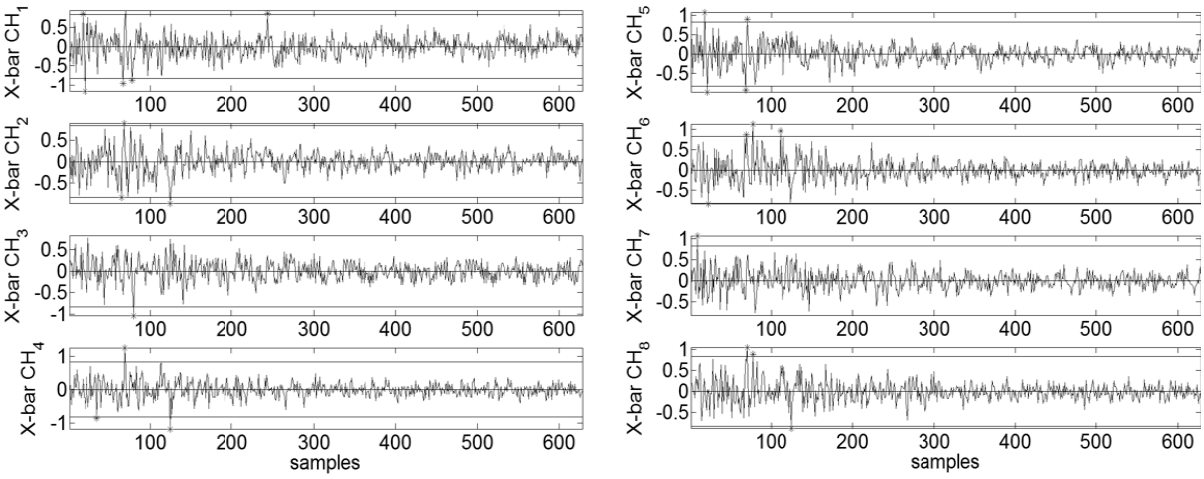

Fig. 17 X-bar control charts for the residuals in the RC case.

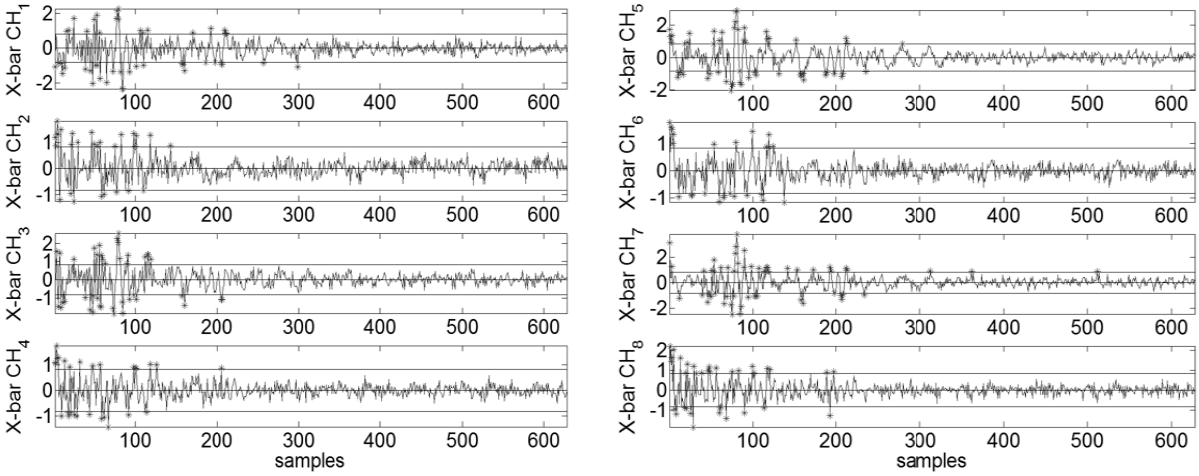

Fig. 18 X-bar control charts for the residuals in the DC case.

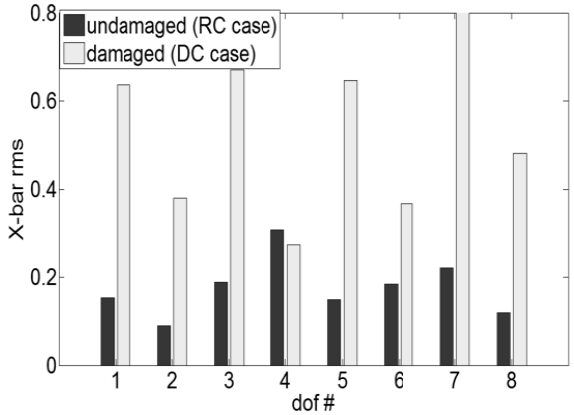

Fig. 19 Rms values computed for each dof on the X-bar charts, in the RC case and DC case.

be noted along the 2nd, 6th and 8th dofs. It can be concluded that the results presented in Fig. 19 indicate that the most damaged direction of the building is the y-direction, in agreement with the results obtained from the previous methods.

- S control chart

The S charts for all the channels show the same properties of the X-bar charts and are not reported here for brevity. For each S chart, the root mean square of the deviations between the upper outliers and the UCL and of those between the lower outliers and the LCL are presented in Fig. 20. Here, the rms values for all the dofs are higher in the DC case than in the RC case, but nothing can be said about the damage position and the most damaged direction of the building, since both the rms values for each case and the gaps between the DC and RC

cases are comparable for all the dofs. Hence, in this case, it is concluded that, using the S control chart, it is only possible to confirm the presence of the damage since it is reflected in different values of the rms between the RC and the DC cases. This makes the S rms an index that is less reliable than the X-bar rms.

- R control chart

Similar conclusions to those for the S control charts can be drawn for the R control charts. In fact, looking at the root mean square of the deviations on the R chart, as shown in Fig. 21, the same features shown in the previous figure appear: (1) the rms values for all the dofs are higher in the DC case than in the RC case, and (2) no indication is provided about the damage position and the most damaged direction of the building, since both the rms values and the difference between the DC and RC cases have comparable values for all the dofs. As for the S control chart, also the use of the R control chart can only confirm the presence of the damage but it is unreliable in localizing the damaged area in a structure.

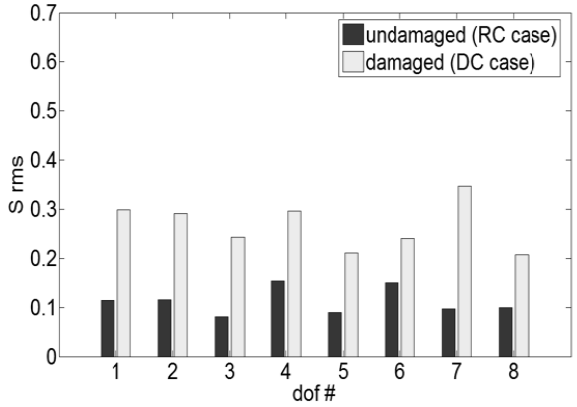

Fig. 20 Rms values computed for each dof on the S charts, in the RC case and DC case.

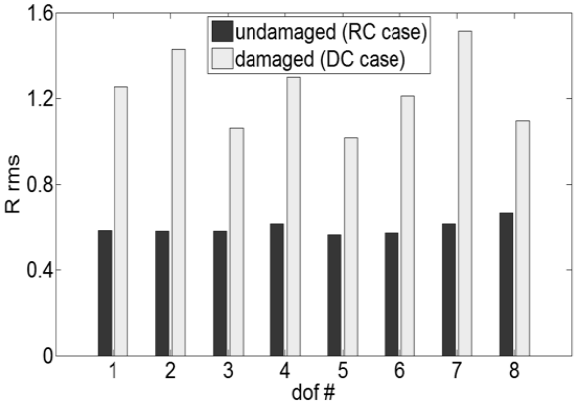

Fig. 21 Rms values computed for each dof on the R charts, in the RC case and DC case.

- False-positive testing

Fig. 22a, Fig. 22b and Fig. 22c show the rms of the deviations for the X-bar, S and R charts, respectively,

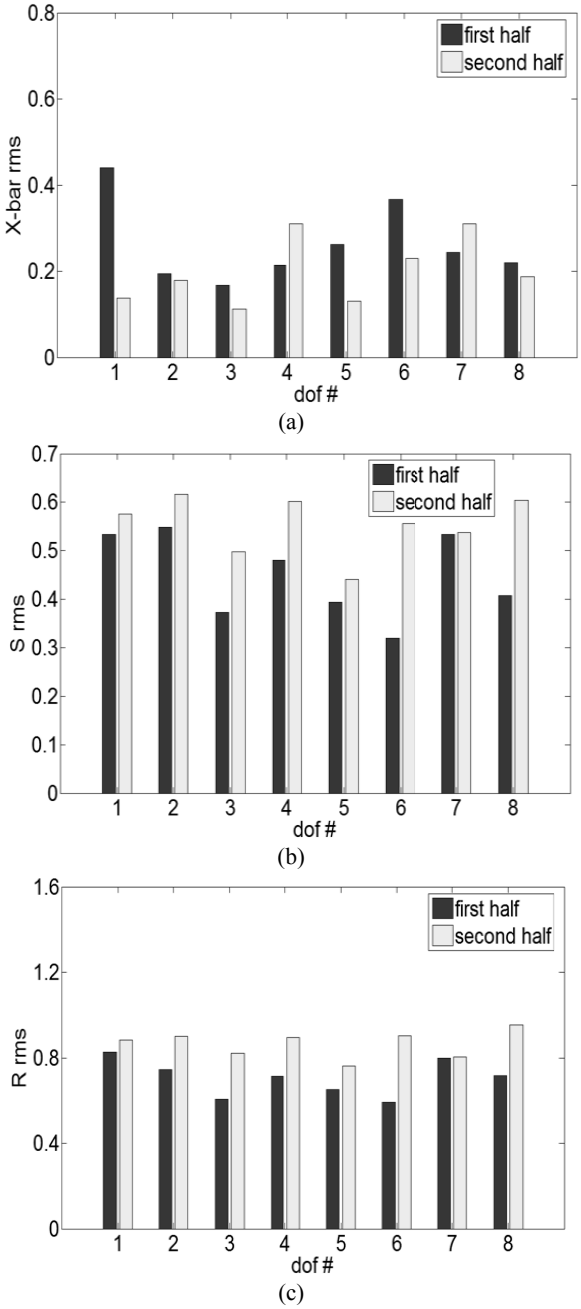

Fig. 22 Rms values computed for each dof, for the first and the second half: (a) on the X-bar charts; (b) on the S charts; (c) on the R charts.

for each dof and for the first and the second half of the signals. For applying the the false-positive testing, the model order and the number of subgroups are chosen to be 500 and 2, respectively, to take into account the reduced size of the signals. Fig. 22 looks different from the previous ones (Figs. 19–21). In fact, in Fig. 22, the difference between the two bars is in average small and can be considered due to the natural variability of the experimental data. This small difference is more evident in the X-bar rms plot, while, in the other two plots, the difference is larger and the bar corresponding to the second half of the signal is always higher than the one for the first half. This indicates that the X-bar chart is the most robust of the three charts against false-positive indications of damage.

4. Conclusions

This paper presents a comparative analysis of some state-of-art vibration-based damage detection approaches with the aim of investigating their efficacy when applied to damage detection of *real world* structures and field measurements and, also, of testing their sensitivity to the presence of structural damage.

In particular, model based and data-driven damage detection methods were reviewed and applied to two case studies: (1) a laboratory scaled four-story steel frame subjected to shake table tests, and (2) a seven-story reinforced concrete building (of Civil and Environmental Engineering Department at NCHU) in Taiwan, subjected to the 1999 Chi-Chi Earthquake and its fore- and aftershocks. In the laboratory structure, damage was simulated by introducing a 66% reduction of the cross-section of one column between the 2nd and 3rd floors, inducing a 22.2% reduction of the inter-story stiffness between these two floors in the weak bending direction. The *real world* structure, the reinforced concrete building in Taiwan, was instrumented for strong motion monitoring with 29 accelerometers and, then, was subjected to the 1998 and 1999 Taiwan Chi-Chi Earthquakes and experienced some structural damage.

With regard to the laboratory structure, it was shown that the analysed model based indexes provided a correct assessment about the presence and/or the location where damage has occurred in the frame. However, no clear indication was given by these indexes in the identification of the amount of the structural damage. Similar conclusions can be drawn for the statistics based indexes which gave a clear indication about the position of the damaged floor in the frame.

For the seven-story reinforced concrete building, the model based indexes clearly identified the most damaged floors and the direction along which damage occurred but, on the basis of the available instrumentation, did not allow to detect the precise position of the damage. Not all the statistics based indexes proved to be reliable in detecting the damage location for this case study.

It is possible to conclude that the model based damage indexes are reliable in the damage detection process for both the laboratory and the *real world* cases. However, they require a sufficient number of sensors to retrieve a complete set of modal parameters and this could be too demanding in *real world* structures which are generally instrumented by a limited number of sensors. The data-driven statistics based indexes are proved to be not accurate in locating damaged areas especially for the *real world* structure. However, they should still be considered since, being non-deterministic, allow to account for the inherent uncertainties in the experimental and field data used in vibration-based damage detection processes.

Structural damage detection in *real world* structures is a complex problem and certainly needs further developments. Based on the results discussed above, it is suggested to compare the results obtained from different damage detection approaches and, also, investigate on the possibility to combine them in order to have a more reliable identification of damage for *real world* cases. By now there are some interesting contributions based on the algorithm fusion approach and we think that this should be one of the research topics to be considered in the future research on structural damage detection.

Acknowledgements

The authors would like to thank Mr. Adrian Brügger (Columbia University) and Dr. C. C. Lin (NCHU) for providing the recorded time histories for the laboratory frame and CEED building. Their help and support in analysing the data is strongly appreciated.

References

[1] S. Alampalli and T. G. H. Cioara, Selective random decrement technique for processing bridge vibration data, in: S. Alampalli (Ed.), Proceedings of Conference on Structural Materials Technology IV, Technomic Publishers: Lancaster, 2000, pp. 75–80.

[2] A. Alvandi and C. Cremona, Assessment of vibration-based damage identification techniques, Journal of Sound and Vibration 292 (1–2) (2006) 179–202.

[3] K. F. Alvin, A. N. Robertson, G. W. Reich and K. C. Park, Structural system identification: From reality to models, Computers and Structures 81 (12) (2003) 1149–1176.

[4] Y. Bai and T. Keller, Modal parameter identification for a GFRP pedestrian bridge, Composite Structures 82 (1) (2008) 90–100.

[5] L. R. Barroso and R. Rodriguez, Application of the Damage Index Method to phase II of the analytical SHM benchmark problem, in: Proceedings of the 15th ASCE Engineering Mechanics Conference, Columbia University, New York, NY, USA, 2002.

[6] D. Bernal, Load vectors for damage localization, Journal of Engineering Mechanics 128 (1) (2002) 7–14.

[7] R. Brinker, L. Zhang and P. Andersen, Modal identification of output-only systems using frequency domain decomposition, Smart Materials and Structures 10 (3) (2001) 441–445.

[8] D. Capecchi and F. Vestroni, Monitoring of structural systems by using frequency data, Earthquake Engineering and Structural Dynamics 28 (5) (1999) 447–461.

[9] F. Cavalieri, M. Imbimbo, R. Betti and A. Brügger, Damage detection of a steel frame subjected to ground motion, in: Proceedings of IOMAC'09 – 3rd International Operational Modal Analysis Conference, Portonovo (AN), Italy, 2009.

[10] F. Cavalieri, M. Imbimbo, R. Betti and C. C. Lin, Dynamic identification and damage detection of a RC building subjected to earthquake excitation, in: Proceedings of the 4th International Conference on Structural Health Monitoring on Intelligent Infrastructure (SHMII-4), Zurich, Switzerland, 2009.

[11] P. J. S. Cruz and R. Salgado, Performance of vibration-based damage detection methods in bridges, Computer-Aided Civil and Infrastructure Engineering 24 (1) (2009) 62–79.

[12] A. Deraemaeker and A. Preumont, Vibration-based damage detection using large array sensors and spatial filters, Mechanical Systems and Signal Processing 20 (7) (2006) 1615–1630.

[13] S. W. Doebling, C. R. Farrar, M. B. Prime and D. W. Shevitz, Damage identification and health monitoring of structural and mechanical systems from changes in their vibration characteristics: A literature review, LA-13070-MS, UC-900, Los Alamos National Laboratory: Los Alamos, NM, 1996.

[14] S. W. Doebling, C. R. Farrar and M. B. Prime, A summary review of vibration-based damage identification methods, Shock and Vibration Digest 30 (2) (1998) 91–105.

[15] G. Fraraccio, A. Brügger and R. Betti, Identification and damage detection in structures subjected to base excitation, Experimental Mechanics 48 (4) (2009) 521–528.

[16] M. Fraser, A. Elgamal, X. He, J. P. Conte, Sensor network for structural health monitoring of a highway bridge, Journal of Computing in Civil Engineering 24 (1) (2010) 11–24.

[17] M. I. Friswell and J. E. Mottershead, Finite Element Model Updating in Structural Dynamics, Kluwer Academic Publishers: Dordrecht, 1996.

[18] M. L. Fugate, H. Sohn and C. R. Farrar, Vibration-based damage detection using statistical process control, Mechanical Systems and Signal Processing 15 (4) (2001) 707–721.

[19] J. He, Damage detection and evaluation I, in: J. M. M. Silva and N. M. M. Maia (Eds.), A Chapter in Modal Analysis and Testing, Kluwer Academic Publishers: Dordrecht, 1999, pp. 325–344.

[20] X. He, B. Moaveni, J. P. Conte, A. Elgamal and S. F. Masri, System Identification of Alfred Zampa Memorial Bridge Using Dynamic Field Test Data, Journal of Structural Engineering 135 (1) (2009) 54–66.

[21] L. U. C. Hermans and H. V. D. Auweraer, Extraction and validation of structural models from tests under operational conditions, in: Proceedings of Symposium on International Automotive Technology, SIAT/SAE Technical Paper Series: Pune, India, 1999, pp. 293–302.

[22] A. L. Hong, R. Betti and C. C. Lin, Identification of dynamic models of a building structure using multiple earthquake records, in: Proceedings of International Symposium on Structural Control and Health Monitoring, Taichung, Taiwan, 2008.

[23] S. A. Jang, S. H. Sim and Jr B. F. Spencer, Structural damage detection using static strain data, in: Proceedings of World Forum on Smart Materials and Smart Structures Technology '07(SMSST'07), Chongqing and Nanjing, China, 2007.

[24] J. N. Juang, Applied System Identification, Prentice Hall, 1994.

[25] G. Kerschen, K. Worden, A. F. Vakakis and J. C. Golinval, Past, present and future of nonlinear system identification in

structural dynamics, Mechanical Systems and Signal Processing 20 (3) (2006) 505–592.

[26] J. T. Kim and B. J. Park, Vibration-based damage monitoring in model plate-girder bridges under uncertain temperature conditions, Engineering Structures 29 (7) (2007) 1354–1365.

[27] C. G. Koh, Damage detection of buildings: Numerical and experimental studies, Journal of Structural Engineering 121 (8) (1995) 1155–1160.

[28] K. Y. Koo, S. H. Sung, J. W. Park and H. J. Jung, Damage detection of shear buildings using deflections obtained by modal flexibility, Smart Materials and Structures 19 (11) (2010) 115026.

[29] J. Kosmatka and J. M. Ricles, Damage detection in structural modal vibration characterization, Journal of Structural Engineering 125 (12) (1999) 1384–1392.

[30] P. L. Liu, Identification and damage detection of trusses using modal data, Journal of Structural Engineering 121 (4) (1995) 599–608.

[31] B. Moaveni, X. He, J. P. Conte, J. I. Restrepo and M. Panagiotou, System identification study of a seven- story full-scale building slice tested on the UCSD-NEES shake table, Journal of Structural Engineering 2010.

[32] B. Moaveni, X. He, J. P. Conte and J. I. Restrepo, Damage identification study of a seven-story full-scale building slice tested on the UCSD-NEES shake table, Structural Safety 32 (5) (2010) 347–356.

[33] K. K. Nair, A. S. Kiremidjian and K. H. Law, Time series-based damage detection and localization algorithm with application to the ASCE benchmark structure, Journal of Sound and Vibration 291 (1–2) (2006) 349–368.

[34] A. K. Pandey and M. Biswas, Experimental verification of flexibility difference method for locating damage in structures, Journal of Sound and Vibration 184 (2) (1995) 311–328.

[35] S. K. Panigrahi, S. Chakraverty and B. K. Mishra, Vibration-based damage detection in a uniform strength beam using genetic algorithm, Meccanica 44 (6) (2009) 697–710.

[36] Y. C. Pati and P. S. Krishnaprasad, Rational wavelets in model reduction and system identification, in: Proceedings of the 33rd Conference on Decision and Control, Lake Buena Vista, Florida, USA, 1994.

[37] C. Ratcliffe, D. Heider, R. Crane, C. Krauthauser, M. K. Yoon and J. W. Jr. Gillespie, Investigation into the use of low cost MEMS accelerometers for vibration-based damage detection, Composite Structures 82 (1) (2008) 61–70.

[38] M. Rucka and K. Wilde, Application of continuous wavelet transform in vibration-based damage detection method for beams and plates, Journal of Sound and Vibration 297 (3–5) (2006) 536–550.

[39] S. Saitta, P. Kripakaran, B. Raphael and I. F. C. Smith, Feature selection using stochastic search: An application to system identification, Journal of Computing in Civil Engineering 24 (1) (2010) 3–10.

[40] J. S. Sakellariou and S. D. Fassois, Stochastic output error vibration-based damage detection and assessment in structures under earthquake excitation, Journal of Sound and Vibration 297 (3–5) (2006) 1048–1067.

[41] O. S. Salawu and C. Williams, Bridge assessment using forced-vibration testing, Journal of Structural Engineering 121 (2) (1995) 161–173.

[42] Z. Y. Shi, S. S. Law and L. M. Zhang, Structural damage localization from modal strain energy change, Journal of Sound and Vibration 218 (5) (1998) 825–844.

[43] H. W. Shih, D. P. Thambiratnam and T. H. T. Chan, Vibration-based structural damage detection in flexural members using multi-criteria approach, Journal of Sound and Vibration 323 (3–5) (2009) 645–661.

[44] W. J. Staszewski, Structural and mechanical damage detection using wavelets, The Shock and Vibration Digest 30 (6) (1998) 457–472.

[45] N. Stubbs, J. T. Kim and K. Topole, An efficient and robust algorithm for damage localization in offshore platforms, in: Proceedings of ASCE 10th Structures Congress, San Antonio, Texas, USA, 1992.

[46] M. M. Waheb and G. D. Roeck, Dynamic testing of prestressed concrete bridges and numerical verification, Journal of Structural Engineering 3 (4) (1998) 159–169.

[47] L. Wang and T. H. T. Chan, Review of vibration-based damage detection and condition assessment of bridge structures using structural health monitoring, in: Proceedings of the Second Infrastructure Theme Postgraduate Conference: Rethinking Sustainable Development — Planning, Engineering, Design and Managing Urban Infrastructure, Queensland University of Technology, Brisbane, Australia, 2009.

[48] Y. L. Xu, J. Zhang, J. C. Li, Y. Xia, Experimental Investigation on Statistical Moment-based Structural Damage Detection Method, Structural Health Monitoring 8 (6) (2009) 555–571.

[49] Y. J. Yan, L. Cheng, Z. Y. Wu and L. H. Yam, Development in vibration-based structural damage detection technique, Mechanical Systems and Signal Processing 21 (5) (2007) 2198–2211.

[50] J. Yu, M. De Angelis, R. Betti and M. Imbimbo, Damage detection in reduced order models of linear structural systems, in: Proceedings of the 4th International Workshop on Structural Health Monitoring 2003, Stanford, California, USA, 2003.

[51] J. Yu, M. Imbimbo and R. Betti, Identification of linear structural systems with a limited set of input-output measurements, ASME Journal of Applied Mechanics 76 (3) (2009) 031005.